1

CLIMATE & ENVIRONMENTAL MODELLING

Capacity to model and forecast climate and environmental processes at different spatio-temporal scales has the potential to revolutionize our approach and ability to address many issues that concern us closely. It was to address these issues in an integrated manner and to generate a capability for multiscale forecasting that CEMP was initiated.

Inside

A: Climate Variability, Climate Change and Sustainability

Sustainability in a changing climate is a critical issue for our times and is the focus of the supra-institutional project under the 11th Five Year Plan. In this Report we present results that have implications at regional to local scales.

A.1 The Shrinking Indian Summer Monsoon

The Indian summer monsoon plays a critical role in India's economy. In the backdrop of a changing climate, we investigate whether the Indian summer monsoon is changing either in terms of duration or spatial coverage. Such an analysis specifically for the continental Indian region has both conceptual and societal implications, and has been lacking. We show here, based on an analysis of daily gridded observed rainfall data for the period 1951–2003, that there are decreasing trends in both early and late monsoon rainfall and number of rainy days, implying a shorter monsoon over India. Similarly, there is a sharp decrease in the area that receives a certain amount of rainfall and number of rainy days during the season. As mentioned above, one possibility is an increase (decrease) in the amount of rainfall or the number of rainy days during the pre-June period, signifying an effective increase (decrease) in the rainy season.

Examination of the amount of rainfall and the number of rainy days over Kerala (72.5 - 77.5°E; 8.5 - 15.5°N) in the pre-onset (May 15-May 31) period, however, shows only a decreasing trend (figure 1a, top and bottom panels respectively). A similar analysis over central India (70.5 - 80.5°E; 17.5 – 35.5°N) for the (post-withdrawal) period (September 15-October 10) also shows significant decreasing trends (figure 1.1b, top and bottom panels respectively). Thus there is no early onset, while the monsoon is shrinking in terms of withdrawal. For the pre-June period, the decrease in the area-averaged rainfall and the number of rainy days are 59% and 47%, respectively of the mean values. For the post monsoon period the corresponding values are smaller (39% and 24%, respectively) but still significant.

Even though the total monsoonal rainfall (June-September) for the country may not change significantly due to a complex combination and spatial distribution of trends, the area (number of grid points) that receive current mean monsoonal rainfall may change.

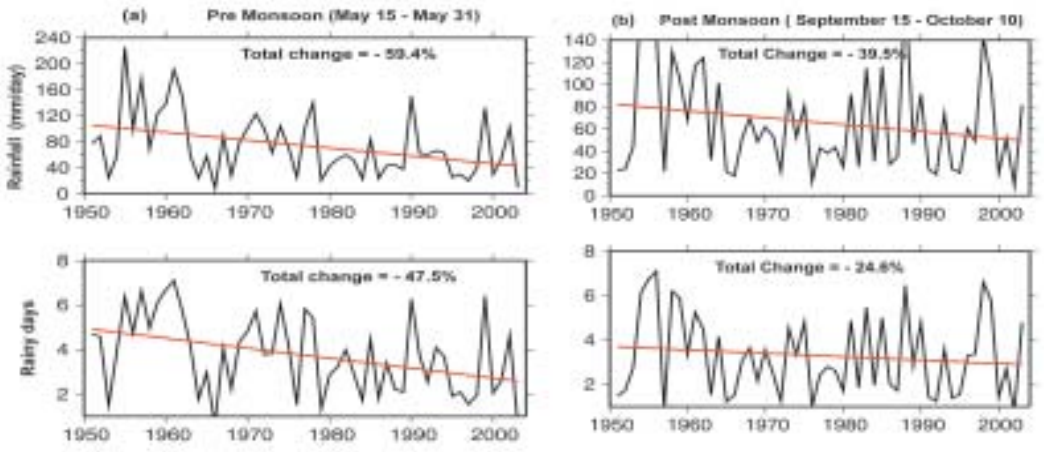

Figure 1.1 Linear least square trends in (a) pre monsoon (May 15-May 31) rainfall (mm/year, top panel) and number of rain days (greater than 5 mm/day, bottom panel) over Kerala (72.5°E-77.5°E and 8.5°N-15.5°N) based on 53 years of gridded daily rainfall data from India Meteorological Department (IMD). (b) post monsoon (September 15-October 10) rainfall (mm/year, top panel) and number of rain days (greater than 5 mm/day, bottom panel) over central India (70.5°E-80.5°E and 17.5°N-35.5°N) based on 53 years of gridded daily rainfall data from IMD.

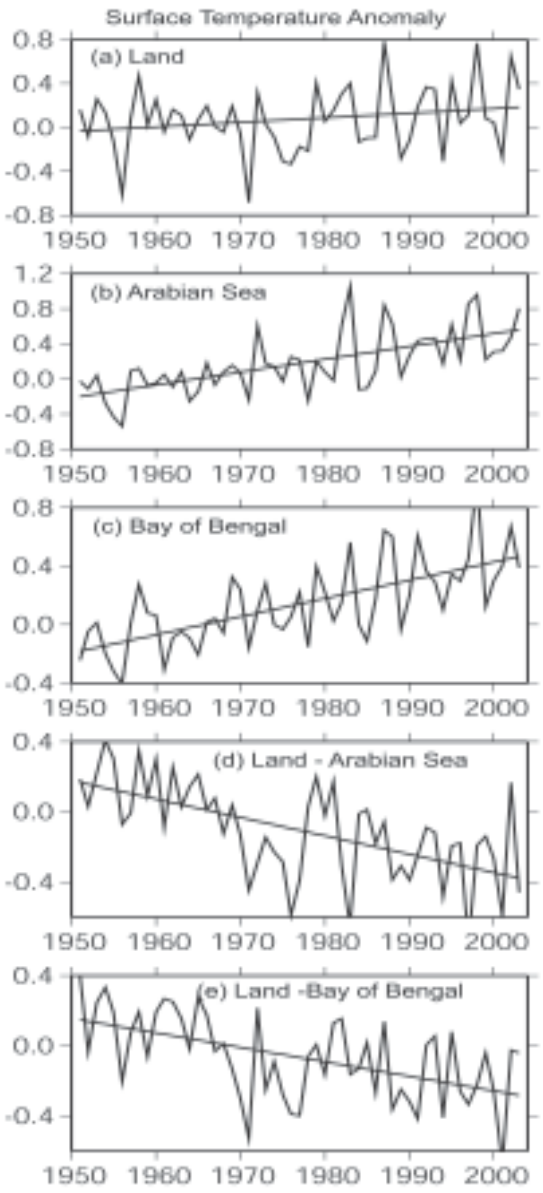

Figure 1.2 Inter annual variability and linear trend in the area averaged surface temperature Indian land mass (a) and the two ocean basins (b&c) during 1950-2003. The bottom panel show interannual variability and linear trend in the contrasts in surface temperatures between land and ocean.

In terms of spatial coverage, that receives the current mean seasonal rainfall and the current mean number of rainy days (24-hour rainfall >= 5 mm), however, there are significant decreasing trends. Similarly, number of grid points (% of area) that receive rainfall or number of rainy days one standard deviation below the 53-year seasonal mean are increasing. In terms of amount of rainfall, this shrinkage is as much as 30% between 1950 and 2003, while the corresponding shrinkage in terms of number of rainy days is close to 40%.

However, one reason why the pre-onset and post-withdrawal rainfall may not be increasing in spite of an increasingly warmer environment (ocean) could be found in the tremendous spatial inhomogenity in the trends in surface temperature. Although there are warming trends over both the ocean basins and the Indian land mass, there are significant differences in the trends. This results in a reduced land-ocean temperature contrast (figure 1.2), which can weaken the strength of organized convergence over India. Thus even if the average trend in surface temperature over the Indian ocean is positive, the spatial distribution of trends does not encourage spatially coherent warm SST or the organized dynamics necessary for the monsoon.

K V Ramesh and P Goswami

A.2 Carbon Fluxes in India and Central Asia

This collaborative project between C-MMACS - IIA, Bangalore and LSCE, France, CaFICA sponsored by the Indo-French Centre New Delhi, is designed to quantify a major uncertainty in the climate controlling parameters: global carbon fluxes, that is, the amount of carbon exchanged at various sites on the globe and in different seasons between the atmosphere, and the oceans or land underneath. This element of the global carbon cycle remains an outstanding quantity as yet poorly resolved, that is responsible for the wide divergence in modeled projections of future increases in the global temperature. Our project is designed to estimate the space-time distribution of these fluxes by exploiting the formulation that atmospheric CO_2

concentrations C (X*,T*) at a site X* at time t*, can be expressed as a convolution between global fluxes F_{kj} ($X_{k,}$ t_j) at sites $X_{k,}$ and times t_j,

and the atmospheric Green's function $G(X^*,t^*,X_k , t_j)$. The fluxes can therefore be estimated from atmospheric concentrations C (X*,T*) measured at various sites X* at times t*, by deconvolving from these, the atmospheric Green's function through a process of Inversion, but makes exacting demands on the precision (100 ppb) of C (X*,T*) to be so inverted.

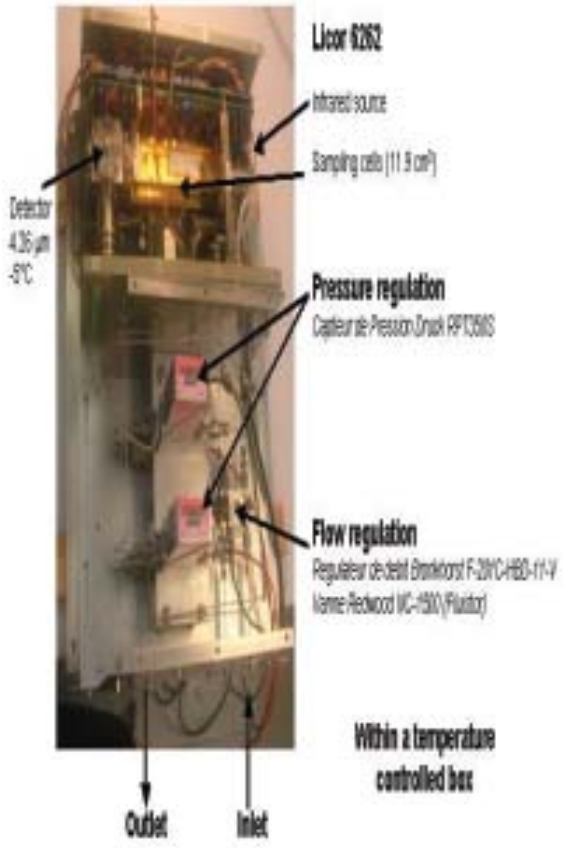

Figure 1.3 Regulations of the inlet flow, the inlet pressure, and of the Licor temperature

High precision monitoring of atmospheric CO_2 still represents a challenge. The international monitoring network is made of about 30 observatories, located mostly in Europe and North America. In addition to these sites, where CO_2 is measured continuously, there are about 70 locations where air is sampled once a week. The samples are analyzed in central laboratories located in Europe, North America, Japan and Australia. Over Asia, however, regional variations in atmospheric CO_2 concentrations are monitored at very few sites.

The principal objective of the CaFICA project was the development of the measuring system and the inverse model needed for such an approach in India.

A major achievement of the CaFICA project has been the establishment of a very high precision CO_2 analyzer at the Indian Astronomical Observatory site in Hanle, Ladakh. This remote location, at an elevationof 4562 m above sea level, already furnished with considerable infrastructure, was selected to provide a background site which will serve as a reference for the Indian network. The objective was to build an instrument dedicated to continuous CO_2 measurements with a precision of 100 ppb as recommended by the World Meteorological Organization (WMO/ GAW). Since an instrument of the desired precision was unavailable off the shelf, a specially designed microprocessor based environment developed at LSCE and DAPNIA/ CEA, was adopted for the purpose.

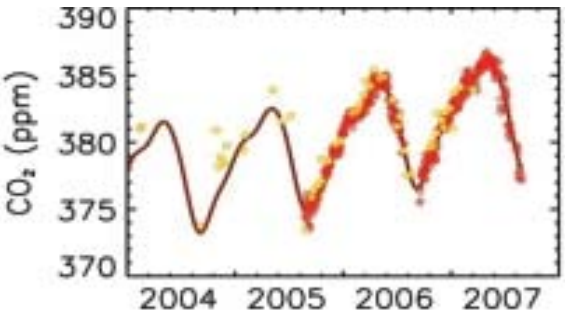

Figure 1.4 Atmospheric CO2 at Hanle form flask (yellow) and in-situ (red) measurements.

Atmospheric CO_2 concentrations measured at Hanle using flask samples since 2003, and CARIBOU since September 2005, are shown in Figure 1.4. Typical hourly measurements over a one week period are shown in Figure 1.5 a and diurnal cycles of CO_2 residuals, wind profile in Figure 1.7b. This analyzer includes;

A pumping and drying unit that samples the air at a flow rate of 5 litres/min to allow a permanent flush of the inlet line. Because

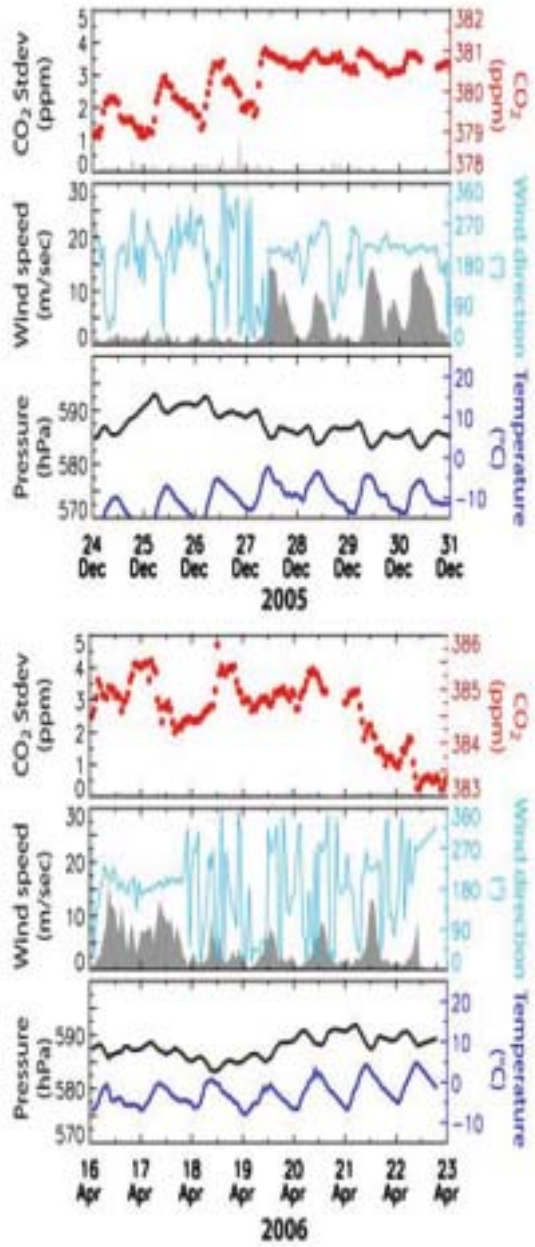

Figure 1.5 (a) Typical hourly measurements over a one week period.

water vapour absorbs infrared radiation at the wavelength used by this analyzer LICOR, we dry the air, using a cryocool unit at a temperature of -60°C.

A calibration unit that links the CO_2 observed mixing ratios to the international calibration scale. This calibration scale is used every 8 days to determine the non- linear response of the analyser. To determine and correct the instrument drift, one reference gas is injected for 10 min in the sample cell once per hour. After this correction the residual drift is as low as 1 ppb per day. Finally, for quality control, a target gas is injected as a regular air sample every day allowing for monitoring of the instrument performance and long-term stability.

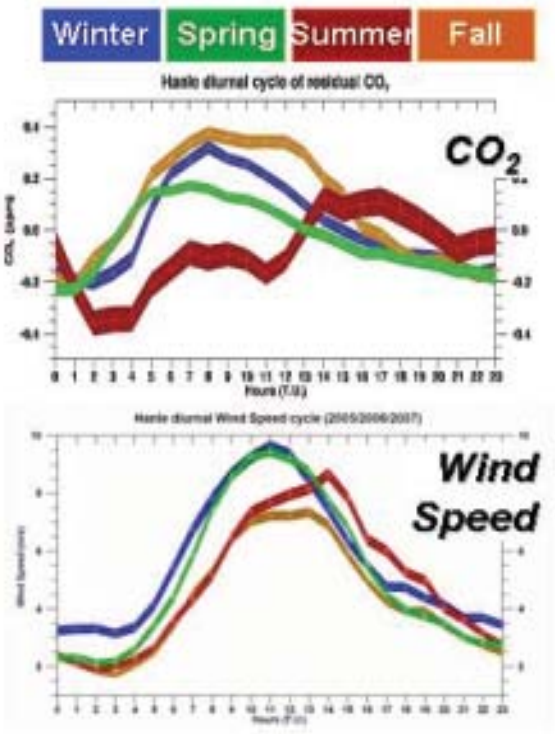

Figure 1.5 (b) Diurnal cycles of CO_2 residuals, wind speed, wind direction, and temperature averaged for the four seasons over the period 2005-2007.

A measurement unit that reproduces CO_2 measurements depends on the quality of temperature, flow and pressure regulations; we have reached a CO_2 reproducibility of 17 parts per billion.

The CARIBOU, the flow in the sample and reference cells (20± 0.005 ml/min), and the cell pressure (660± 0.04 mbar) are controlled using fuzzy logic algorithms.

A transmission unit handles the transfer and storage of data. The Hanle Caribou station has its own control system. A network link allows remote supervision, configuration and maintenance. The raw data are downloaded automatically every day or more frequently if

needed by a central computer located at LSCE and at the Hoskote Centre of IIA, Bangalore, which also allows for database operations.

V K Gaur, B C Bhatt and Michel Ramonet

A.3 CO_2 Measurement and Analysis

C-MMACS and IIA has been engaged in the operation of in-situ CO_2 analyser at Hanle. In addition we have installed an air sampling system at Hanle observatory and at Pondicherry in collaboration with the Pondicherry University. The objective is to sample air every week in 1Lt glass flasks, according to a protocol to minimize contamination from local emissions. A large part of the international monitoring network is made of such sampling programs, which can be easily deployed without large local infrastructure. Even though the resolution is not as good as the continuous analyzers (especially due to the low temporal resolution of the data set), flasks sampling programs are very important by providing measurements of several trace gases (CO_2, CH_4, N_2O, SF_6, CO).

The samples are analysed at LSCE, which is linked to the international network by regular inter-comparisons with 5-6 other central analytical facilities. Measurements of CO_2 in the flasks sampled at Hanle, provides a quality control of the in-situ measurements (Figure 1.6). Analysis of other species will enable us to monitor the trends of CH_4 and N_2O, two greenhouse gases emitted by specific processes (e.g. rice paddies, biomass burning, fertilizers, etc.) which are important in India.

Measurements of trace gases like CO, SF_6 and CO_2 isotopes can be used to understand the major processes responsible for the observed variations of greenhouse gases. At the moment we have analyzed about 9 months of flasks sampled at the new site of

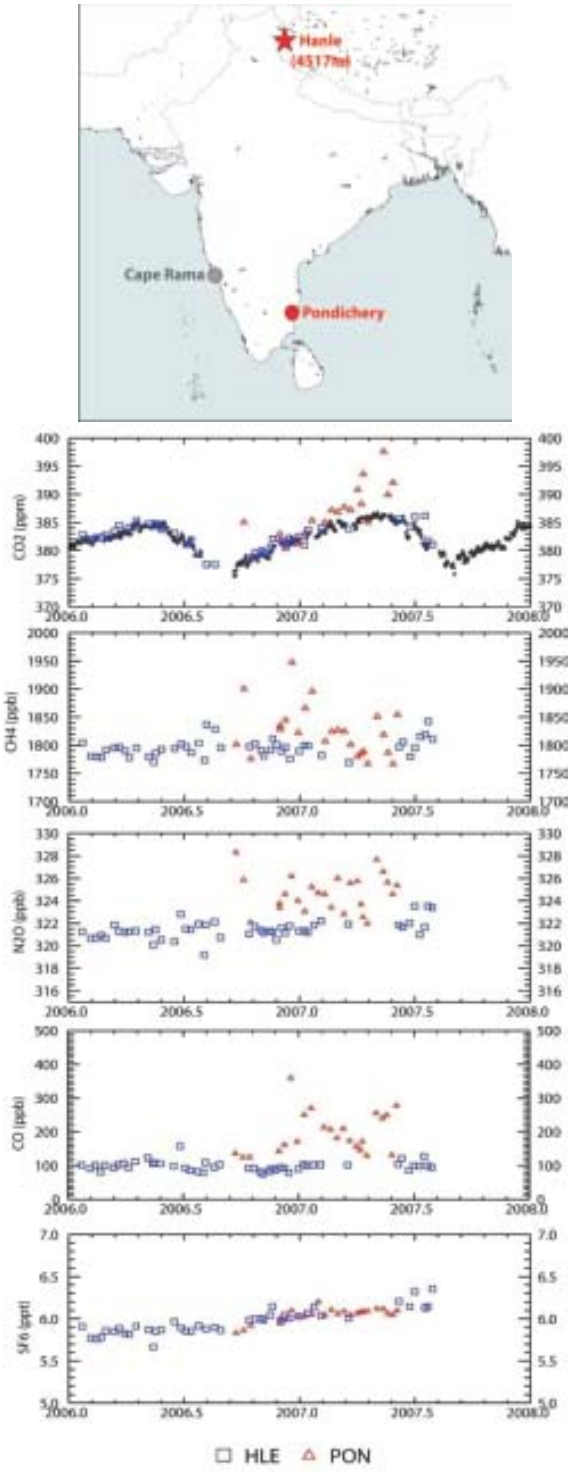

Figure 1.6 Measurements of CO_2, CH_4, N_2O, CO and SF_6 from flasks sampled at Hanle (blue) and Pondicherry (red). In-situ CO2 measurements at Hanle are shown in black.

Pondicherry. The comparison of measurements at Hanle and Pondicherry is displayed in Figure 1.3 which already shows interesting features. For almost all the species the concentrations observed at Pondicherry are higher than the ones observed at Hanle.

This positive offset at Pondicherry is related to the contribution of regional emissions in South India. The 100ppb offset for CO is due to the important contribution of biomass for cooking and heating. Surprisingly there is no difference in SF6 at these two sites. This greenhouse gas has no natural source, and is used as an insulator in electrical transformers, in double glazing, and specific industrial processes. In Europe and North America SF6 can be used as a tracer of emissions from cities. In the present case, it appears that there is no emission of SF_6 in Pondicherry area, and consequently the concentrations of this trace gas are as stable as in the remote site like Hanle.

The combined in-situ and grab samples CO_2 time series from Hanle is shown in Figure 1.7. The preliminary results have been presented at the 14th WMO/IAEA Meeting of Experts on Carbon Dioxide, Other Greenhouse Gases, and Related Tracer Measurement Techniques, in Helsinki, and a publication is in preparation.

The typical CO_2 diurnal cycle is characterized by amplitude of about 0.5 ppm (Figure 1.5b). It is maximum in Winter/Fall, with highest CO_2 concentration observed during the afternoon. The CO_2 daily maximum corresponds to a period of increase of the wind speed from 2-3 m/s up to 7-10 m/s. At the same time there is also a shift in wind direction from 160° to 210°. In summer the CO_2 diurnal cycle presents a first plateau in afternoon, and a highest one between 8pm and midnight. Such CO_2 variability, clearly linked to the local meteorology, implied that the representation of CO_2 concentrations is different from daytime to night time. This is a typical feature observed at mountain stations. However, due to the low density of CO_2 local sources around Hanle observatory, the difference of concentration remains very low and consequently all valid data are considered as representative of large scale surface fluxes.

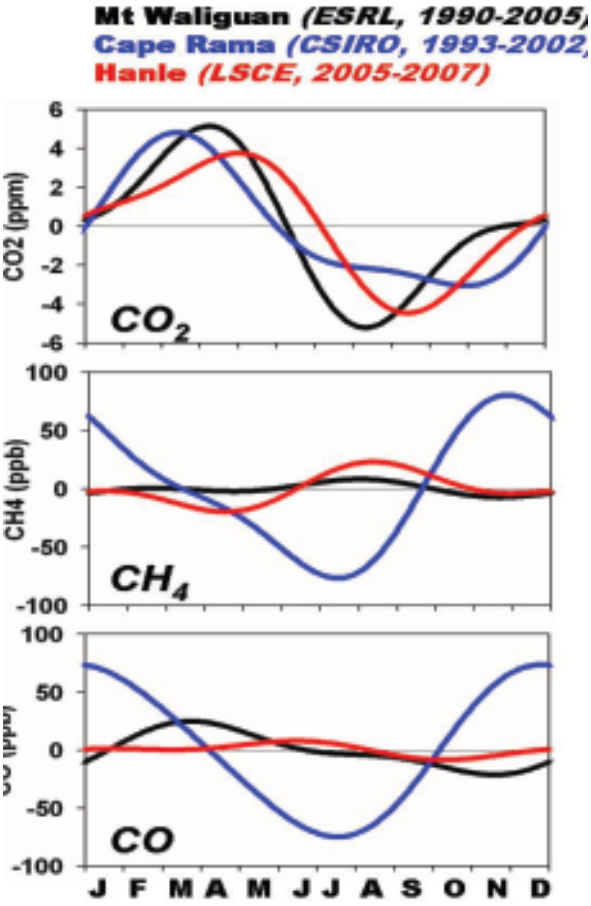

Figure 1.7 Mean seasonal cycle of CO2 (above), CH4 (middle) and CO (below) estimated from measurements at MtWaliguan (black), Cape Rama (blue) and Hanle (Red).

There are very few trace gases monitoring sites located in India and Central Asia, and consequently it is difficult to make a comparison of regional gradients. We have used existing observations of CO_2, CH_4, CO from Mt Waliguan (China) and Cape Rama (India) obtained from flask sampling program established respectively by NOAA/ESRL and CSIRO, to compare with the measurements at Hanle. We have calculated the mean seasonal cycles from the detrended measurements. The period of observation is different for each site, and is significantly shorter at Hanle compared to the two other sites. The in-situ CO_2 measurements at Hanle show a shift of about one month in the spring drawdown

(Figure 1.7). The differences between the coastal site of Cape Rama and the two other sites are more significant for CH_4 and CO.

For both species the Cape Rama data set shows a seasonal cycle with amplitude of about 150 ppb, much higher than in Hanle and Mt Waliguan. The observed gradients can be explained by the monsoon circulation

Indian summer monsoon takes place from June to September with prevailing winds from the southwest, whereas the winter monsoon winds blow from the northeast. Consequently, in summertime Cape Rama experiences marine air masses and minimum pollution level. The CO_2 miminum appears truncated because the air masses originated from southern hemisphere have a smaller biospheric signal. At the same time the air sampled at Hanle has flown over India, inducing a maximum level of CH_4 concentration in September. No similar maximum is observed for CO. In winter the circulation patterns is reversed and maximum levels of CH_4 and CO are observed at Cape Rama, as a result of the regional Indian emissions.

N K Indira, P S Swathi, V K Gaur, B C Bhatt, and Michel Ramonet

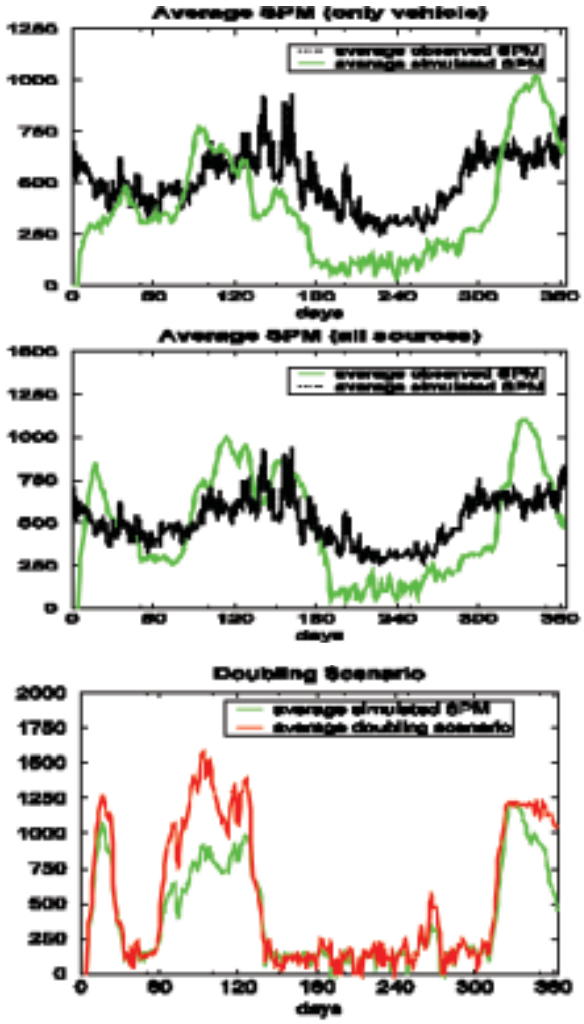

Figure 1.8 Average values (2000-2005) of observed (black dotted line) and simulated (green line) for SPM over Delhi as indicated.

A.4 Simulation of Daily Variation of Suspended Particulate Matter over Delhi:

The massive growth in the size and the population of cities over the past few decades has led to serious deterioration in the quality of air. One of the important constituents of air borne pollutants which is a major health hazard, is suspended particulate matter (SPM).

Effect of traffic congestion (doubling of idling time and doubling of total number of vehicles).The red line represents projected average (2000-2005) daily SPM if the total number of vehicles and the idling time were doubled. The corresponding standard simulations (green line) are presented for comparison. The meteorological variables have been adopted from NCEP daily Reanalysis over 2.5×2.5 box over Delhi. The observed data is from CPCB.

SPM is also an important source of cloud condensation nuclei, accurate simulations of SPM with sufficiently long lead thus have many applications, from issuing health advisories to forecasting fog. One of the biggest challenges in modeling air pollution in general and SPM in particular, is to identify and mathematically represent the (location-specific) sources and sinks. In this study we present a dynamical

model for daily values of SPM over Delhi. The meteorological parameters are taken from the daily values from NCEP Reanalysis. The validation is carried out against observations generated by the Central Pollution Control Board, India (CPCB) for the period 2000-2005. Error statistics show that the model can capture a significant part of the observed variability of SPM. An evaluation of the relative contributions of various sources show that while vehicular pollution accounts for a large fraction of the SPM throughout the year, steep increases in the winter and the pre-monsoon periods are accounted for by fossil fuel burning and wind blown dust, respectively. Simulation with a doubling scenario for traffic congestion shows the effect to have strong seasonality. Such a model can be also interfaced with a seasonal forecast model or a climate model for enhanced scope of seasonal forecasts or investigation of impact of SPM on regional climate change.

P Goswami and J Baruah

A.5 Parameter Sensitivity Analysis for the Coupled Physical-Biological-Chemical Model in the Indian Ocean

Parameter sensitivity studies have been carried out using a 3D coupled physical-biological-chemical model. This marine ecosystem model is evaluated by using US JGOFS data, WOCE data, satellite data and buoy data for different values of a few of the parameters which influence the regeneration of ammonium and growth of zooplankton and hence the carbon flux across the air-sea interface.

In these simulations, spatial and temporal variations of Chlorophyll (Chl), Primary Productivity (PP), Zooplankton (Z) and Bacteria (B) are examined in detail for the Arabian Sea (AS) and the Bay of Bengal (BOB). On a basin-wide scale, high PP and Chl in North-Western

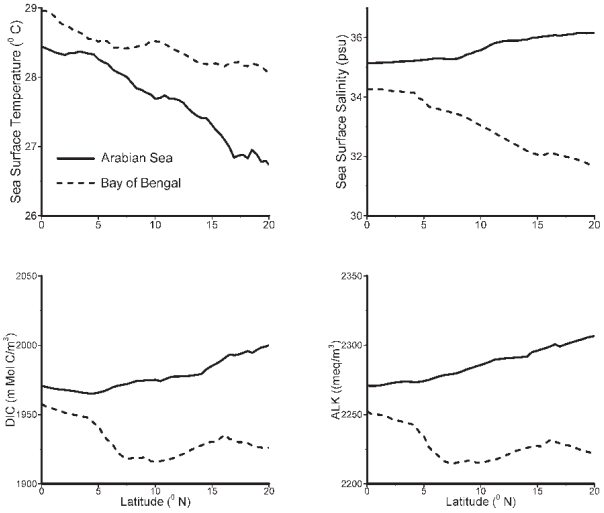

Figure 1.9 DIC (mmolC/m³) and ALK (meq/m³) along the 9°N transect in the Arabian Sea and along the 10°N transect in the Bay of Bengal in the upper 500m

AS and southern coast of India in all the seasons are seen both in observations and models.

One of the numerical experiments (expI), succeeds best in capturing low PP and Chl during SIM, regions of high PP and Chl during SWM, NEM and FIM in AS and BOB.

The chemical variables Dissolved Inorganic Carbon (DIC) and Alkalinity (ALK) obtained from expI for the zonal transect along 9°N in the AS and 10°N in the BOB during September upto 500m depth are compared with observations of WOCE I1 cruise (Figure 1.9). They compare quite well, especially in the upper ~200 meters, with WOCE I1 data.

Variation of annual mean of zonally averaged temperature, salinity, DIC and ALK in the top 20 meters with latitude in AS (42-78°E) and in BOB (78-100°E) also shows significant zonal contrast between the AS and the BOB in surface physical and carbon variables throughout the year and the zonal contrast increases with latitude (Figure 1.10). Higher SST, lower salinity and DIC of surface water translate into generally lower pCO_2 in the BOB than in the AS.

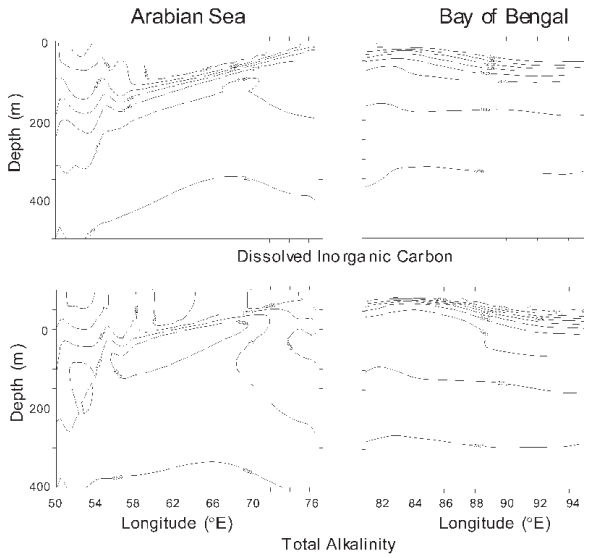

Figure 1.10 Meridional variation of zonal averages in SST (°C), Salinity (psu), DIC (mmolC/m³) and ALK (meq/m³) between the Arabian Sea (42-78°E) and the Bay of Bengal (78-100°E)

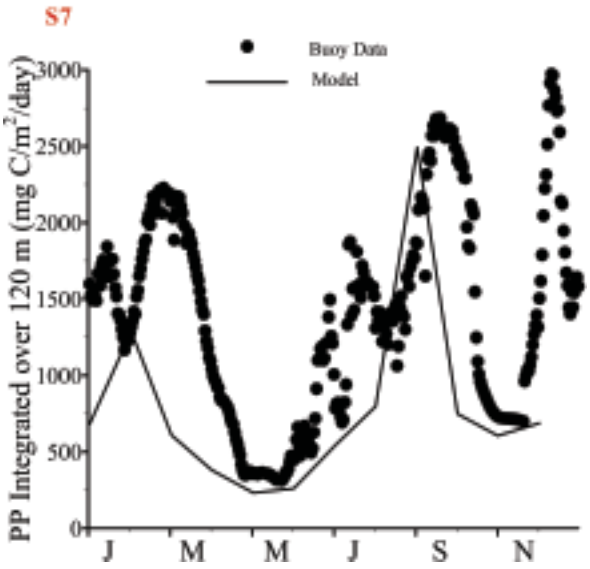

Figure 1.11 Seasonal variation of Depth Integrated Primary Productivity (mg C/m²/day) compared with Buoy Data at S7 in Arabian Sea for the new coupled physical- biological-chemical model for the Indian Ocean.

Spatial and seasonal variations of all source and sink terms of chemical variables, dissolved inorganic carbon and alkalinity, are being studied in detail for four numerical experiments to understand the effect of parameters on the air-sea carbon flux.

A new biological model having two currencies Nitrogen and Carbon, is incorporated into new version of Modular Ocean Model (MOM4). The ecosystem model consists of Phytoplankton, Zooplankton, Bacteria, Ammonium, Nitrate, Trichodesmium, Detritus, Labile and Semilabile Dissolved Organic Matter. In this model, dissolved organic matter is modeled in detail and variable Chl:C ratio for photosynthesis, and variable C:N ratio for all state variables of the ecosystem is used.

Several simulations of this coupled model are carried out by varying the values of model parameters. It was found that spatial and temporal variation of PP integrated over the euphotic zone obtained from one of the simulations agrees well with PP derived from SeaWiFS data. Also, PP from this model simulation compares well with the cruise data at a few stations in AS and buoy data at S7 in AS during NEM, FIM and early SWM (Figure 1.11).

P S Swathi, M K Sharada and K S Yajnik

A.6 Semi-annual Periodicity in the Tropical Indian Ocean

A simple exact method has been developed to analyze ocean climatology to highlight the characteristic property of the tropical Indian Ocean, namely, semi-annual periodicity by splitting seasonal anomaly into a semi-annually periodic component and its orthogonal complement.

Analysis of seasonal thermal cycle by applying the method to World Ocean Atlas 2005 dataset (WOA2005) shows a significant semi-annual oscillation especially in the North Indian Ocean. Its key mechanism, it is hypothesized, is the quadratic dependence of mass transfer coefficient on the surface wind speed that generates even harmonics. The hypothesis is tested with a free-surface Indian Ocean General Circulation Model based on Modular

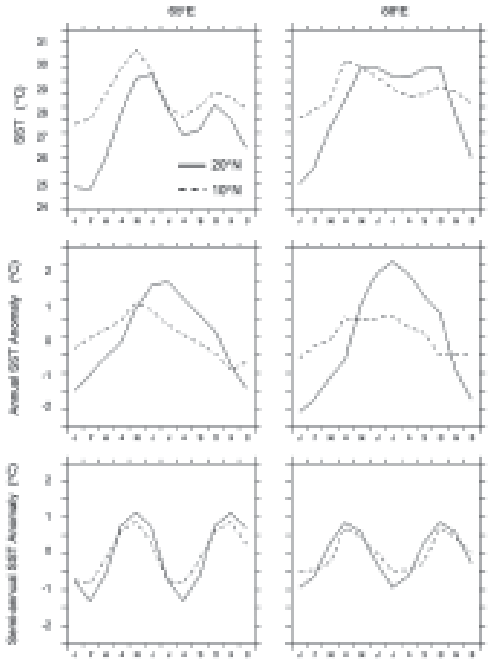

Figure 1.12 Sea surface temperature (SST), its annual anomaly and its semiannual anomaly at 10°N and 20°N on the 65°E transect in the Arabian Sea and the 88°E transect in the Bay of Bengal. Data from World Ocean Atlas 2005

Ocean Model (MOM4) after validating it rigorously with WOA 2005. The results have been submitted for publication.

K S Yajnik, M K Sharada and P S Swathi

A.7 Comparison of Mixed Layer Depth with Triton Buoy Observations

We have taken up this study for understanding mixed layer variability on different time-scale (intraseasonal to interannual) using OGCM simulations after validation against available insitu observations.

Global ocean model simulations have been used in the present study to simulate the thermal structure and mixed layer variability of the Indian Ocean. The ocean model used is the latest version of Modular Ocean Model-4 (with various fluxes) and has a sea-ice interface developed by Geophysical Fluid Dynamics Laboratory (GFDL), Princeton. The domain of the model is 180°W-180°E and 80°S-80°N with a horizontal resolution of 1°. There are 50 levels in the vertical with 20 levels in the upper 150 m.

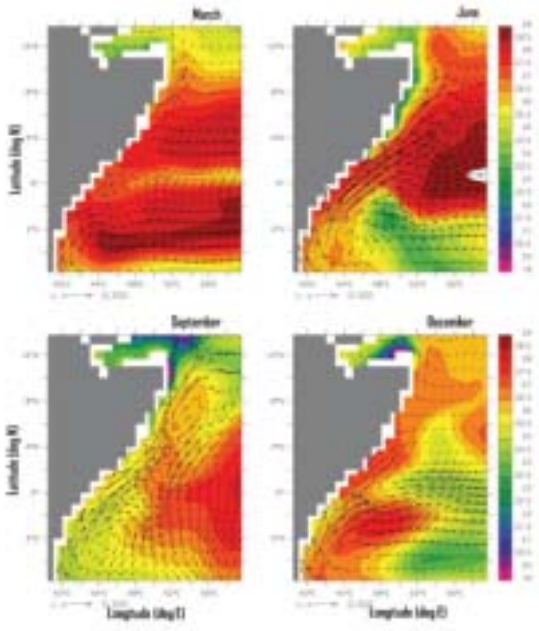

Figure 1.13 Seasonal variation of monthly SST (deg C) for Somali Current system in (a) March (b) June (c) September (d) December at a depth of 50 m overlayed with current vectors.

The model was spun up 15 years using climatological forcing along with various fluxes. Then we have used the simulations of the 20th year for the study of various features. Figure 1.13 shows the model derived sea surface temperature (SST) along with ocean currents for various seasons along the Somali coast.

The model simulated MLD is compared against available insitu observations from Argo floats and Triton moored buoys. At one of the Triton

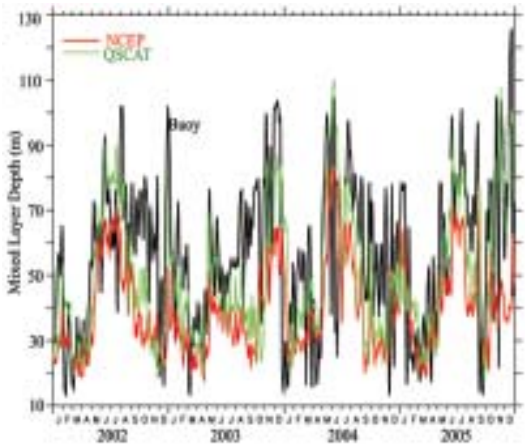

Figure 1.14 Comparison of model simulated mixed layer depth (5-day averages) with computed MLD from the TRITON buoy observations (90°E and 1.5°S).

buoy locations (90°E and 1.5°S), we have compared the model simulated mixed layered depth (using two momentum forcings, NCEP and quickSCAT winds) with observations. Though the model is able to pickup trends (Figure 1.14) of shallowing and deepening there are considerable differences during monsoon season (JJAS). The reason for the lack of agreement between model simulations and observations at the buoy point is the spatio-temporal separation. The observations are at a point location whereas the model is the representation of the grid around the point.

C Kalyani Devasena and P S Swathi

B. Forecast and Analysis of Indian Summer Monsoon

Improved scope and skill of monsoon forecasting along with better understanding of the physical processes that given the monsoon dynamics are high-priority research areas at C-MMACS and is an integral part of the supra-institutional project under the 11th Five year Plan.

B.1 Long-range, High-Resolution Forecast of Monsoon:Post-Season Evaluation with Multi-source Analysis

Our basic objective is to develop and evaluate methodology for long-range and high resolution forecasting of monsoon rainfall categories and record it in an objective manner for a systematic evaluation and improvement. Our study shows that significant improvement in skill is possible through careful calibration of the model configuration. The minimum skill here refers to skill attainable using only an AGCM without the interannual variability of SST; this minimum skill thus provides a quantitative benchmark for assessing configurations with added complexity like ocean-atmosphere coupling.

In the present case this calibration has been carried out with respect to model grid, especially in terms of resolution over the monsoon domain, the high resolution ('50 km)

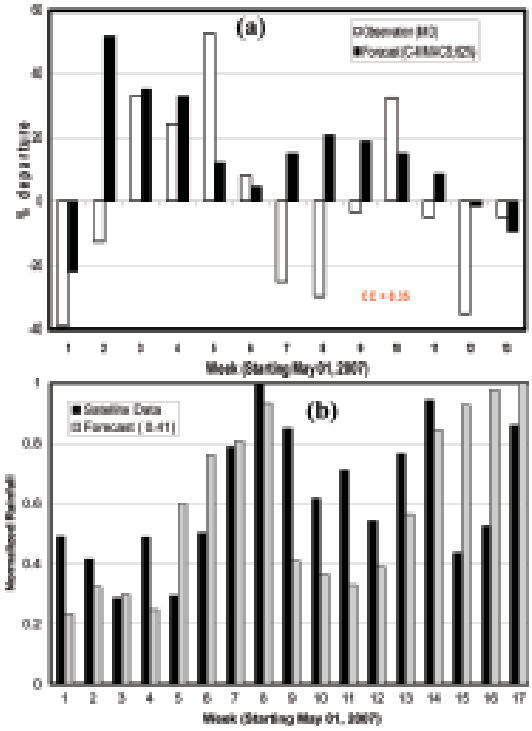

Figure 1.15 (a) Comparison of observed and predicted weekly rainfall anomalies for 2007. The observed anomalies are adopted from IMD (www.imd.ernet.in) and the C-MMACS forecast represents ensemble average of five initial conditions between April 01 to May 01, 2007 from NCEP Reanalysis. The phase (%) and correlation coefficient (CC) are given in the panel. (b) area-averaged (75-85°E, 8-28°N) weekly rainfall normalized with respect to respective maximum value from high-resolution satellite data (hollow bar) and model forecast (filled bar) for 2007. The model forecast represents ensemble average of five initial conditions between April 01 to May 01, 2007 from NCEP Reanalysis. The correlation coefficient between the two time series is given in the bracket.

over the monsoon region has been achieved using a VR GCM to carry out a large number of simulations in a computationally non-prohibitive way.

Since 2003, long-range, high-resolution forecasts of monsoon have been generated and communicated to a wide spectrum of users and institutions including India Meteorological Department (IMD) for objective, post forecast evaluation. We present here an evaluation of our forecast for 2007 monsoon against observation/analysis from three different sources: IMD, NOAA Analysis and high-resolution (~10 km) satellite data (HR) at a number of important spatial and temporal scales.

The anomalies in the all-India rainfall from

forecasts are very close to the observed values. The maximum error (August) is 3%, while the average error in three months is about 1.6%. Further, the forecast anomalies were higher than the observed in July, while the reverse was true for August, indicating that there is no significant bias. However, it may be noted that there are significant errors in terms of amplitudes and the distribution of the anomalies.

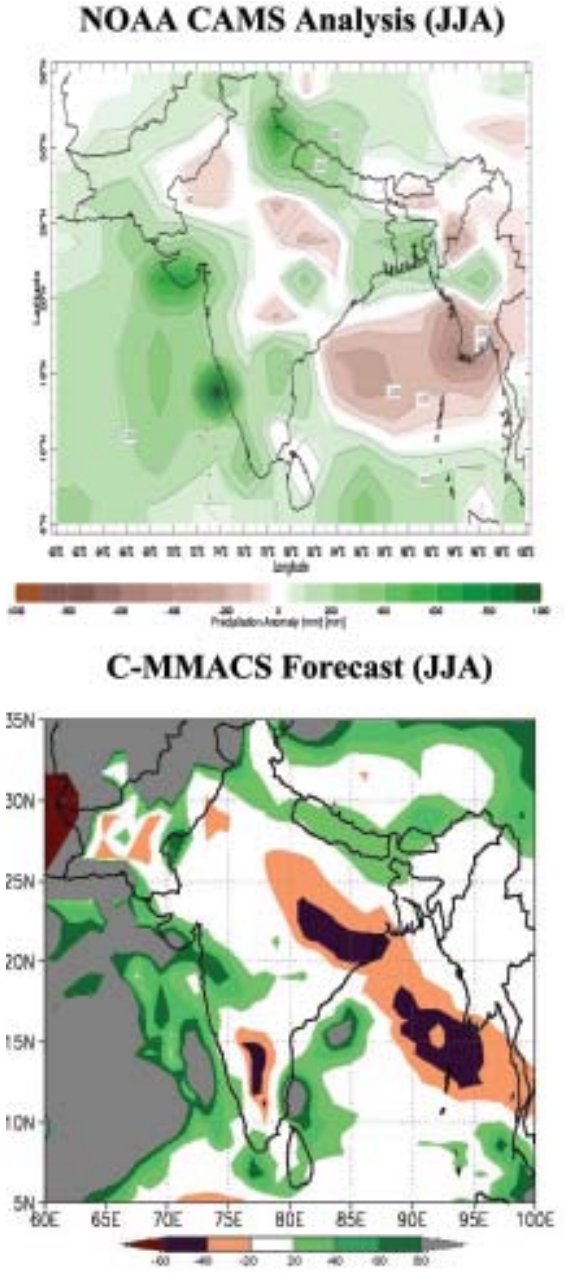

Figure 1.16 Comparison of spatial distribution of seasonal rainfall anomalies in NOAA CAMS analysis (left panel) and C-MMACS model forecast (right panel) for June-August, 2007.NOAA CAMS Analysis C-MMACS Forecast

At weekly scale, the forecast values in anomalies in all-India rainfall show about 62% phase synchronization with the observed (IMD, *www.imd.ernet.in*) values (top panel, figure 1.15). A comparison with the area-averaged (75-85 ^{o}E,8-28 ^{o}N) weekly rainfall from forecast and HRR data shows (bottom panel, figure 1.15) a correlation coefficient of 0.41, which is significant at 95% confidence level for the degrees of freedom involved. While comparing forecasts with HRR data we have normalized each (weekly) data set to its corresponding maximum to bring out the patterns clearly. There are three (beginning 9th) weeks in July where the forecasts show much sharper decrease, while there are two (beginning 15th) weeks in August in which the forecasts do not show the observed decrease. Otherwise, the forecasts follow the observed intraseasonal variability present in HRR data.

It is instructive to compare the C-MMACS forecasts with seasonal anomalies generated by NOAA Climate Anomaly Monitoring System (NOAA NCEP CPC CAMS_OPI V0208 ANOMALY; (http://rain.atmos.colostate.edu/CRDC/datasets/NCEP_CAMSOPI.html). The anomalies are calculated with respect to a base line climatology of Jan 1979 – Dec 2000. The rainfall analysis on a 2.5^{o} X 2.5^{o} global grid is based on rain gauge observation system from CAMS which are merged with precipitation estimates from a satellite algorithm (OPI) shows very good agreement (figure 1.16) not only over India but also over the surrounding region. In particular, the forecast anomalies correctly show the spatial variation over Pakistan, Sri Lanka and Nepal. This hints at the potential of the model for short-term prediction of regional climate.

K C Gouda and P Goswami

B.2 Dynamical Regime of Low Frequency Variability in a Coupled Ocean Atmosphere General Circulation Model

The quasi-periodic change in sea surface temperature (SST) along the equator in the eastern Pacific (with the associated changes in the wind as well as precipitation) goes through warmer or colder phases in the Pacific Ocean is termed as El Nino-Southern Oscillation (ENSO). During the ENSO-years dramatic deviation from the normal course of many climatic phenomenon world over, including the Indian summer monsoon, are observed. However, how does ENSO impact on them and vice versa are yet to be well understood. Therefore, one of the primary goals in climate prediction is to comprehend the dynamical nature of ENSO.

At present there is no consensus on whether the dynamics of observed ENSO falls in a linear regime or in a non-linear one. Some studies argue that ENSO is linear and stable in general; the validity of this statement is questioned only during the peak phases of ENSO. However there are regions in the tropical Pacific where low frequency variability cannot be explained by damped coupled feedbacks and stochastic forcing. This could be attributed to the inherent non-linearity in coupled system in general and in particular to the non-linearity associated with the tropical convection.

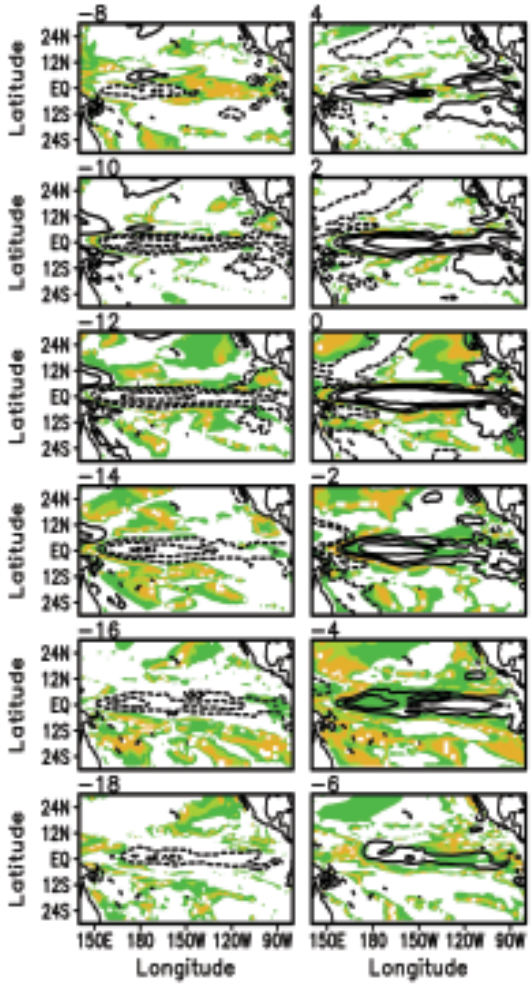

Figure 1.17 The spatial structures (during the different phases the model-ENSO) of composite SST anomaly (contour) and ratio of composite residual to composite SST anomaly (color). The residuals are plotted only when its amplitudes are equal or greater than the 10% of the amplitudes of the local anomaly. The compositing is done base amplitude of Nino-3 SST anomaly. The time indices shown on the top-left side of each panel are relative to the time at which the Nino-3 averaged SST peaks. Thus zero value corresponds to the peak-phase of ENSO and negative and positive values denote different lags and leads (in months) with respect to the peak phase.

This study assesses how well a linear stochastic model reproduces the interannual variability of the tropical Pacific in COLA Anomaly Coupled Ocean and Atmosphere General Circulation Model (C-ACGCM). For this purpose a set of seasonally varying Markov models best fit to 300 years of continuous simulations from C-ACGCM have been used. These Markov models are built in a multivariate (i.e., sea surface temperature, heat content, both the zonal and meridional components of wind stress and total heat flux) empirical orthogonal function (MEOF) space with reduced dimension while retaining the important covariability. These empirical models are trained in the first 300 years and verified in the last 50 years of the data. The Markov model with 8 retained MEOFs shows the best predictive skill of the interannual variability in the ACGCM for up to about a year. It is important to note that the verification of Markov models in the present as well as most of the previous studies is based on the performance of the statistical model predictions in Nino-3 (ie.

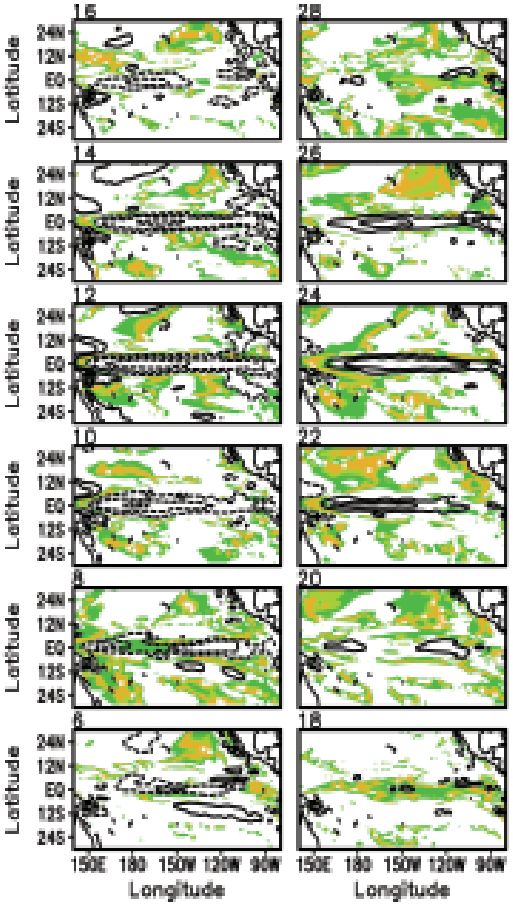

Figure 1.18 Same as figure 1.17 but for subsequent phases of composite ENSO in the model

150°W-90°W, 5°S-5°N) region only. This region is a natural choice, since the predictability of ENSO is of the primary focus. However, an important question is how good a Markov representation of low frequency variability in the ACGCM is in the tropical Pacific region as a whole.

One way of checking this is to examine the spatial and temporal distribution of the residual *i.e* $R(t) = P(t) - M * P(t-1)$. Here $R(t)$ is the misfit, $P(t)$ is multivariate principal components, M is seasonal transition matrix and t indicates time. By construction the magnitude of this one-time-step (i.e., one month) residual should be a minimum relative to those of other higher time-step residuals. To examine the relative magnitude of this residual during the different phases the model-ENSO, the composites of sea surface temperature (SST) and its residual are estimated. The value at each spatial point in these composites is calculated by ensemble average. Each member in the ensemble is selected based on both the phase and amplitude of Nino-3 time series (N3) constructed from the model-SST anomaly. When the maximum amplitude of N3 during October and following April exceeds 0.5°C, a space-time slice of data is selected. Each of these slices is centered on the month when ENSO peaks and covers the data symmetrically 15 months before and after the peak-month. The condition that the events should peak between October and April is imposed to minimize the effect of seasonality on the compositing. Thus, approximately 90 events are selected to estimates the composites. The spatial structures of ratio of the local magnitude of the SST-residue to that of its anomaly during the life cycle of model-ENSO are shown in color in figure 1.17 & 1.18. These figures also show the SST anomaly composites as contour.

The largest misfits are generally in the subtropics. However, there are occasions when the misfits are large near the equator. But the latter is true only in regions where the local SST anomaly is small. In general, a narrow region between 5°S and 5°N in the Pacific Ocean behaves more like a linear model. But in the off equatorial region this linear approximation generally fails. Also note that for the equatorial western Pacific west of 160°E, a region where abundant convective activity occurs both in the model and in nature, it is hard to get any clear picture. Another interesting fact is that during the peak phases of SST anomaly, the amplitudes of the residual are relatively more confined to boundaries of large SST anomaly. In short this analysis hints at the possibility of accommodating the two competing points of views of ENSO into a single framework, by virtue of the fact that both linear and non-linear dynamics seems to operate in

a non-overlapping manner in both space and time.

Center for Ocean-Land-Atmosphere Studies

Rameshan Kallummal and Ben P Kirtman

B.3 Super High Resolution Simulation of Monsoon Climate and its Variability

Tropical convection and its organization on different spatio-temporal scales were analysed using a very high resolution global general circulation model (GCM) developed at Meteorological Research Institute (MRI), Japan. First time, a long climate simulation of a global spectral general circulation model (GCM) at a spatial resolution of ~20-km horizontal mesh (*TL*959*L*60), was performed on the Earth Simulator successfully. Comparison with two lower resolution simulations of 120-km (*TL*159*L*40) and 180-km resolution (*TL*95*L*40) shows that convection, climatological fields and moist stability over the Indian Ocean and SPCZ are better represented in *TL*959*L*60 than in lower resolution simulations.

Figure 1.19a shows mean outgoing longwave radiation (OLR) overlaid with corresponding 850 hPa winds for the winter season from

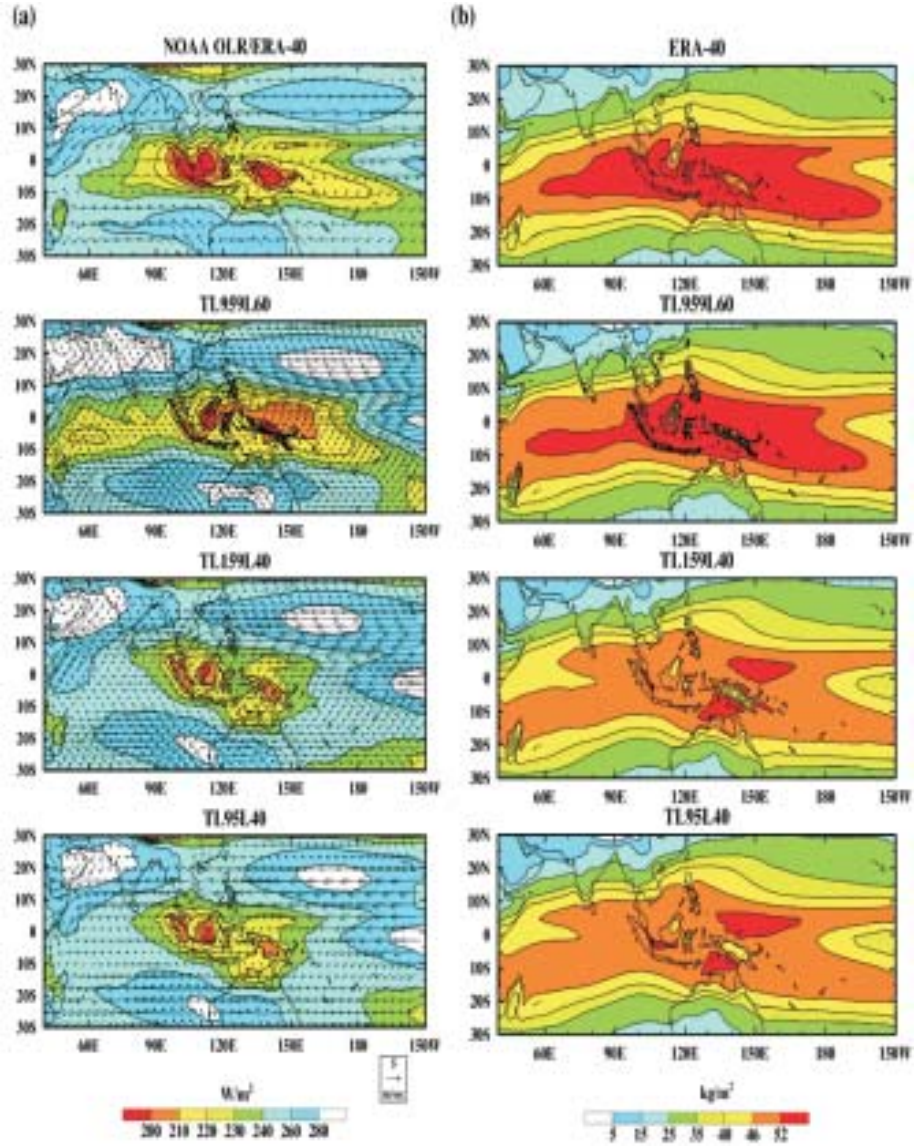

Figure 1.19 (a) Climatological winter mean OLR overlaid with 850 hPa winds and (b) vertical moist stability [VMS, deûned as $GMS_{(400^{\sim}50hPa)}$ - $GMS_{(1000\text{-}400hPa)}$ where GMS is the gross moist static stability] from (i) observation, (ii) TL959L60, (iii) TL159L40, and (iv) TL95L40.

observation and the simulations. Observed OLR indicates convection over equatorial region stretching from Indian Ocean to the dateline including the South Pacific Convergence Zone (SPCZ) roughly from 15S to 10N. In *TL*959*L*60, simulated low OLR is realistic over the equatorial regions of Indian Ocean and the SPCZ but slightly overestimated over the western Arabian Sea.

However, in terms of intensity, location and distribution of convective activity, *TL*959*L*60 tends to give an improved simulation over the observed seasonal convective centers. In *TL*159*L*40 and *TL*95*L*40, the zonal extent of simulated OLR less than 240Wm^{-2} is much smaller and mainly restricted to northern parts of Australia, Indonesia, and the maritime continents of West Pacific. Consistently, in *TL*959*L*60, the strength of the low level circulation and the location of the convergence over major convective centers (equatorial regions of Indian Ocean and the SPCZ) are closer to observation compared to *TL*159*L*40 and *TL*95*L*40.

Although *TL*159*L*40 and *TL*95*L*40 capture the convection and associated low-level circulation with weaker magnitudes over these regions, the convection over the equatorial Indian Ocean and SPCZ are much restricted. The resolution sensitivity is thus most pronounced over equatorial Indian Ocean, the maritime continents of the West Pacific, and SPCZ. Thus, the super high resolution simulation was found to be better in resolving the finer climatological features over Indian Ocean and SPCZ.

Comparing the vertical moist static stability [VMS, the difference between gross moist static (GMS) enthalpy of the lower troposphere (1000 hPa-400 hPa) from that of the upper troposphere (400-50 hPa)], we note that the winter distributions of VMS from observation and the simulations (Figure 1.19b) have the same pattern as the large-scale distribution of the corresponding winter mean organized convection (Figure1.19a). Based on moist static energy budget, increase in convection is associated with increase in atmospheric instability and hence decrease in VMS. The zonally oriented region of maximum instability along 10S is confined to the maritime continents in lower resolution simulations, while it is stronger and extensive across the Asia-Pacific and compares better with observation in *TL*959*L*60.

However, this improvement does not translate into the simulation of intraseasonal variability of tropical convection.

We speculate that this inability is largely due to the fundamental problem of the model in reproducing the vertical structure of heating in the tropics (not shown). Thus, while the very high resolution yields improvements in some aspects of tropical mean convection, these appear to be less important compared to the basic deficiency of parameterized convection in capturing tropical convection and its spatio-temporal variability. This warrants continued efforts to improve model physics, particularly the deep convection for yielding more refined MJO simulation.

K Rajendran, A Kitoh, R Mizuta, S Sajani andT Nakazawa

C: High Impact Weather Events and Variability: Forecasting, Analysis and Observation System Design

With growing economic activities and upcoming megacities many weather events like heavy rainfall and fog have high economic and societal impacts. Ability to forecast them with required resolution, lead and precision are intimately linked to reducing vulnerability, a key element of the supra-institutional project.

C.1 Role of Large-scale Meso-scale Fields in Simulation of Extreme Rainfall Events

In principle, a mesoscale simulation is

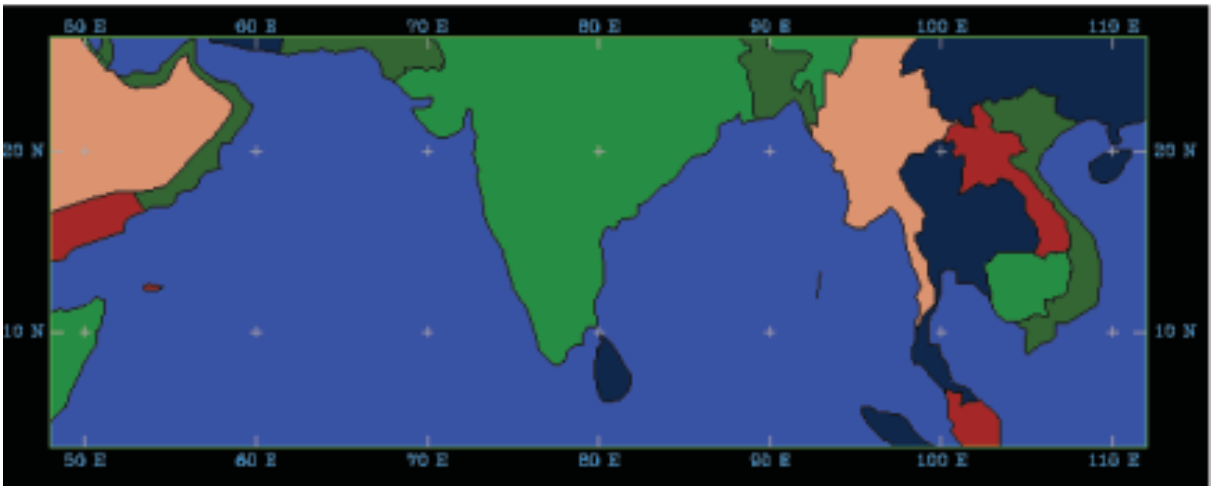

Figure 1.20 The simulation domain used in both control and test runs

expected to be affected by both model dynamics and lateral boundary forcing. The quantitative relative roles of these two factors, however, are not clear. The objective of the present study is to investigate this issue for a given mesoscale event. The mesoscale model MM5V3 has been widely and successfully used in the simulation of intense convective systems. Model results, however, are very sensitive to the choice of domain size resolution, parameterization scheme and also initial fields. One of the necessary requirements in mesoscale simulations to minimize the adverse impact of lateral boundary condition on the model solution is to keep the lateral boundaries away from the region of interest.

Boundary conditions required by mesoscale models have to be generated either from General Circulation Models like forecast. This study is about the impact of two sets of lateral boundary fields on the quality of simulation of the test event. Although fieldslike NCEP reanalysis cannot be used in an actual forecast situation, the hindcast experiments carried out here can provide valuable insight into the role of large-scale fields in simulation of highly localized extreme mesoscale event.

The MM5 model discussed above is used in this study. The model domain shown in Figure 1.20 is selected based on a series of sensitivity studies with different domains (domain calibration), the issue of domain calibration is however not discussed here. The model was configured for single domain with simple ice (microphysics), Anthes-kuo parameterization scheme, 17 vertical levels and NOAH land surface model. Data sets used here, both NCEP 2.5^{o}x2.5^{o}and FNL1^{o}x1^{o}are sourced form http://www.dss.ucar.edu/.

Terrestrial data includes terrain elevation (30-minute), Land-use (USGS-24 Category 30 minute), vegetation fraction (10 minute). Two sets of simulations were carried out : one with FNL 1^{o}x1^{o} (control) and another with NCEP 2.5^{o}x2.5^{o} (test). beginning from 00UTC, 24th July 2005.

Control experiments were carried out with an ensemble size of 5 (test run with one initial condition) and resolution of 30-km. For each of the set mentioned above, the model was integrated for 5 days starting from five different initial conditions 6-hour apart. The heavy rainfall event of Mumbai that occurred during July 26-27th, 2005 was a highly localized event both in space and time; the maximum rainfall of nearly 94 cm was confined to an area of only about 1000 km^{2}, with most of the rainfall occurring in the afternoon of July 26th 2005. However, to account for inherent errors in the

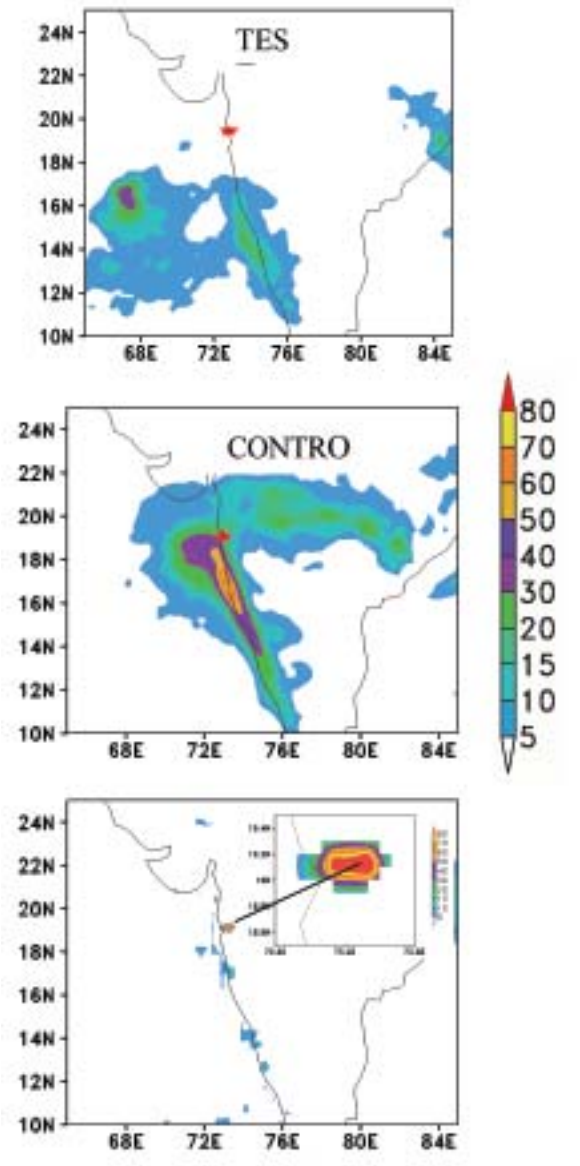

Figure 1.21 Distribution of 30-hour accumulated simulated rainfall using NCEP 2.5°x2.5° (test) and FNL 1°x1° (control) data in cms. The bottom panel shows (10-km resolution satellite data) observed rain in cms during the event. Location of the event (Mumbai) is shown by star.

simulations and a more objective evaluation of domain-wise simulations, we considered a wider area of 2°x2° box centered over the general event location (19°N, 73°E).

Similarly, we have considered a 30-hour time window (26:07:05:06 hour to 27:07:05:12 hour) to evaluate and compare the results. The spatial distribution of 30-hour accumulated ensemble mean rainfall for both test and control simulation along with observed rain (Pingping et al 2002, Goswami and Ramesh, 2006) is shown in Figure 1.21, this figure clearly shows the significant influence of the lateral boundary fields on the mesoscale simulation. In particular, while the control simulation has reasonable success in capturing the event, the test simulation (lateral boundary fields from NCEP 2.5°x2.5 reanalysis) fails both in terms of location and intensity. The control simulation captured spatial structure of the rain quite accurately with the highly localized intense patch (60 to 70 cm) being located around Mumbai.

It is not unexpected that mesoscale simulations are affected by the choice of lateral boundary conditions; our results, however, show that the effect can be profound. While these results need to be substantiated with much larger set of simulations and associated diagnostics , they do however, provide the basis for a more extensive investigation.

S Himesh and P Goswami

C.2 Extreme Rainfall Events and Monsoon Intensity: Quantifying the Role of Synoptic Dynamics

A complete understanding of the spectrum of variability of the Indian summer monsoon (ISM) still remains elusive. ISM is a multi-scale convective system and large-scale processes like sea surface temperature and snow cover as well as convective internal dynamics (CID) play significant roles in its variability; it has been shown that CID can explain the genesis of a wide spectrum of variability, from large-scale intraseasonal oscillations to small-scale synoptic processes. While the role of intraseasonal oscillations in monsoon variability has been examined extensively, an important issue is quantification of the role of synoptic internal dynamics (SID). We address this issue by considering a scenario in which the monsoon rainfall is considered to consist of two parts: a large-scale component controlled by various large-scale processes

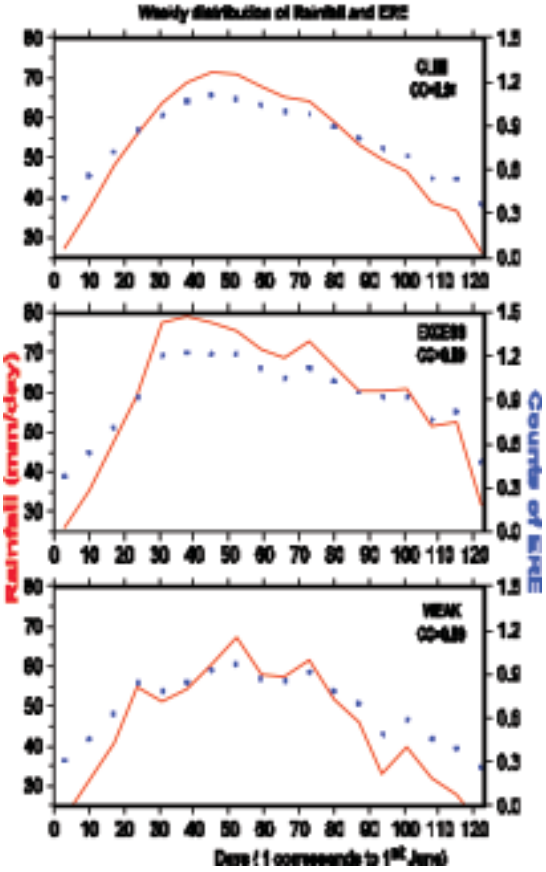

Figure 1.22 Time series of area-averaged weekly rainfall (solid line) and total weekly number of ERE (dash line) over the region (70-85E; 5-30N) averaged over total (top panel), excess (middle panel) and deficit years (bottom panel) for the years 1951-2003. The correlation coefficient between the weekly rainfall and weekly ERE counts for each year is given in the respective panel. The ERE events are based on a threshold intensity of 5 cm/day from the daily gridded data of IMD. The x-axis begins with June 1.

and a component governed by SID and represented by small scale short lived extreme rainfall events (ERE). Based on an analysis with multi-source, independent but compatible datasets we show that SID represented by ERE accounts for about 35% of the variability of ISM.

The association between ISM and ERE exists not only at seasonal scale but also at shorter time scales. Time series of area-averaged weekly rainfall and total weekly number of ERE over the region (70-85E; 5-30N) averaged over total (top panel), excess (middle panel) and deficit years (bottom panel) for the years 1951-2003 shows (figure 1.22) very strong association, with correlation coefficient 0.8 and above. The association between ISM and ERE at weekly scale based on HRR data for the years 2001-2006 show strong correlation between area-averaged daily rainfall and the total number of ERE over that area. Indeed the breaks in the monsoon rainfall often (but not

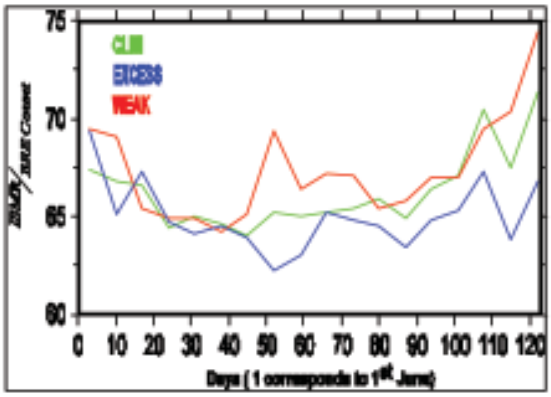

Figure 1.23 Ratio of weekly values of ISMR to the weekly count of ERE for total (green line), excess (blue line) and deficit (red line) years. The ERE events are based on a threshold intensity of 5 cm/day from the daily gridded data of IMD. The x-axis begins with June 1.

always) coincide with the low ERE activity (figure 1.22). The correlation coefficient between the weekly rainfall and the weekly count of ERE given in each panel is highly significant for each year. In fact, there is good correspondence between spatial distribution of anomalies in total rainfall and ERE. It is possible that mechanisms that control large-scale features like northward propagation of monsoon and the monsoon low-level jet also influence the dynamics of ERE.

An intresting insight into the association between ERE and ISM is revealed by an examination of the quantity ; defined

$$\varepsilon = R/N$$

Where R is the total ISMR rainfall and N is the total count of ERE or NRE during the season. The quantity thus represents amount of ISMR rainfall per event. The daily value of for June to September averaged separately over excess, normal and deficit years from IMD data reveals (figure 1.23) shows that follows a distinct seasonal cycle, with highest number

of rainfall per ERE in the early and late monsoon season (figure 1.21), with a minimum in the July – August period. In other words, ISMR is more controlled by ERE during June and September, when the large-scale organized monsoon system is either in the onset or in the retreat phase. Secondly, deficit monsoon years are characterized by higher value of, implying a failure of large-scale organized system characterized by NRE in these years.

P Goswami and K V Ramesh

C.3 Growing Multi-hazard Vulnerability over Northern India

The last few decades have seen rapid, large-scale, and often unplanned urbanization in many parts of the world, especially in India. More than 60% of the world population is projected to be urban by 2020, with India poised to develop a number of mega cities. A serious consequence of such urbanization, and associated land use, is anticipated to be enhanced susceptibility and vulnerability of the population to natural events like earthquakes and extreme weather events like episodes of intense rainfall, especially for areas with high population density.

An interesting feature, important both from the point of vulnerability assessment and observation system design, is revealed by the cumulative geographical distribution of ERE, shown in figure 1.24. The mean geographical location of the monsoon trough is clearly marked by the distribution of ERE. However, ERE of highest intensities are found on the two flanks of the band that marks the monsoon trough. This clearly brings out the distribution of ERE embedded in the monsoon trough. Since the data is at a resolution of 10 km, this distribution of ERE can be used for precision planning of field experiments to study these events.

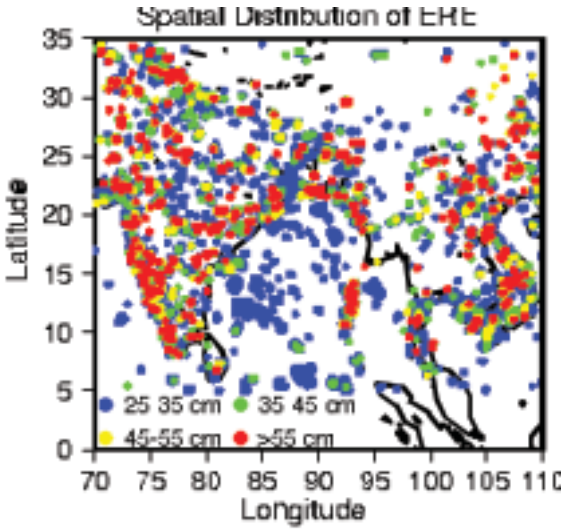

Figure 1.24 Spatial distribution of ERE of different categories accumulated over five years (2001-2005). The high density of ERE over the west coast and along the flanks of the monsoon trough is prominent.

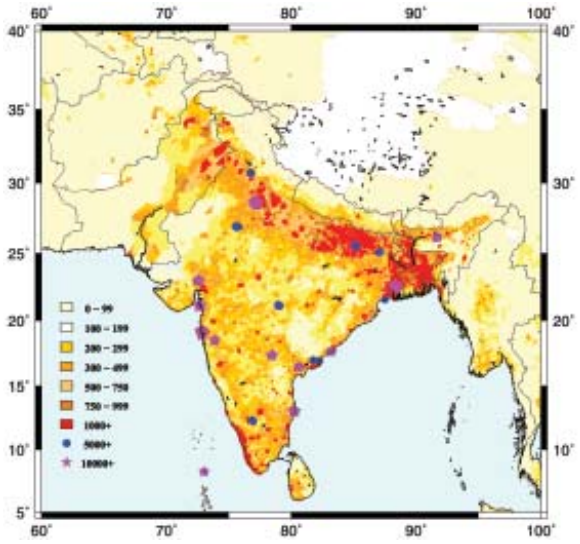

Figure 1.25 Spatial distribution of population density marked with cities and megacities.

A factor that adds to vulnerability of the people to natural events like episodes of heavy rainfall is the increase and redistribution of population. The upper fiit hills of Himalayas, which was only sparsely populated a few decades ago, now have a number of large cities with population exceeding 1000 persons per sq km (figure 1.25). At the same time, many areas in the northern India, including many in the lesser Himalayas, are prone to hyper activity; several of these areas can become hyper arid with an average annual rainfall less than that over Thar

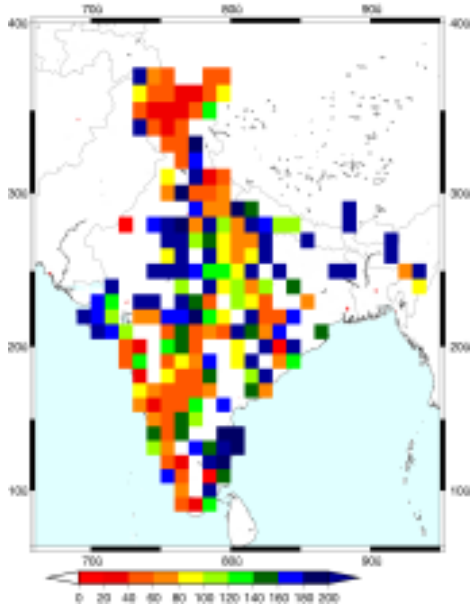

Figure 1.26 Desertification timescale over different parts of India. Desertification timescale is defined as the timescale over which local annual rainfall will fall below the long-period mean over Thar (258 mm) according to local trends in rainfall based on weighted epochal (10-yr) trend ensemble.

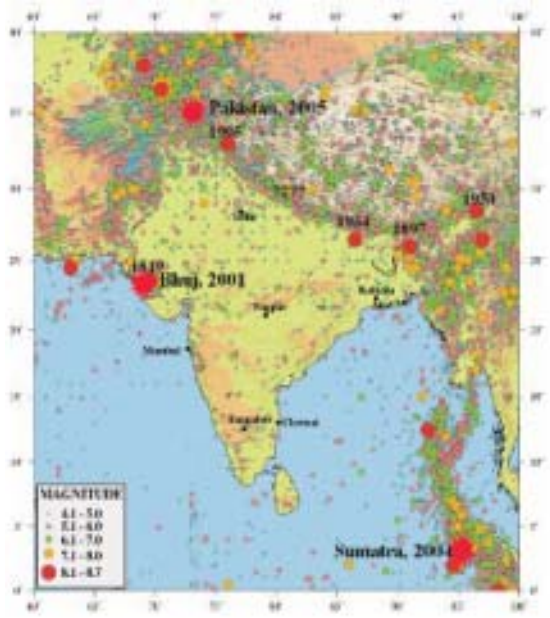

Figure 1.27 Seismicity Map of India

(258 mm) in a time series of less than 50 years (figure 1.26).

The Indian sub-continent is one of the most seismic prone areas of the world. The Himalayan mountains in the north, mid-oceanic ridges in the south and earthquake belts surrounding the Indian plate all show that the

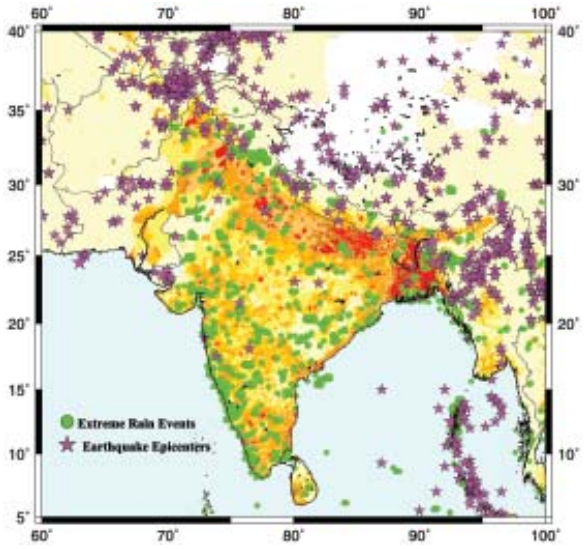

Figure 1.28 Spatial distributions of high intensity earthquake episodes and extreme rain events over India.

sub-continent has undergone extensive geological and tectonic processes in the past. The sub-continent has experienced 13 great earthquakes in the last 200 years of which 5 have occurred within Indian political boundary. Central Himalaya is still considered as seismic gap and such a devastating earthquake is expected any time. Within this decade, this sub-continent has faced Bhuj earthquake, 2001, Sumatra earthquake, 2004 and Pakistan earthquake 2005 caused heavy casualties and severe economic change (figure 1.27).

A composite of Multi-hazard vulnerability can be created by superposing distribution of seismicity and extreme rainfall events over the population growth (figure 1.28). It can be seen that all the three overlaps over the Himalayan belt, marking this belt as a potential zone of natural disasters in the coming years.

P.Goswami, K V Ramesh and I A Parvez

C.4 The C-MMACS Dynamic Fog Forecasting System

Every winter, fog plays havoc through unexpected delays in flights in many airports in India, disrupting important events in industrial and policy sectors. With the many-fold increase

in the volume of air traffic in recent years, for reasons varying from urgent medical help to tourism, any disruption of flight schedule to day affects a large cross-section of the society. Fog, however, also affects a large cross section of the population in many other ways. The protracted fog that covered the Indus and the Gangetic plains in the north and east of the Subcontinent in the winter of 2002-03, for approximately 45 days affected close to 500 million people. Most of the winter vegetables cannot withstand combination of high humidity and low temperature that accompany foggy condition. With the number of foggy days in this region increasing, sometime extending up to a month or more, the vulnerability of these people to fog has increased.

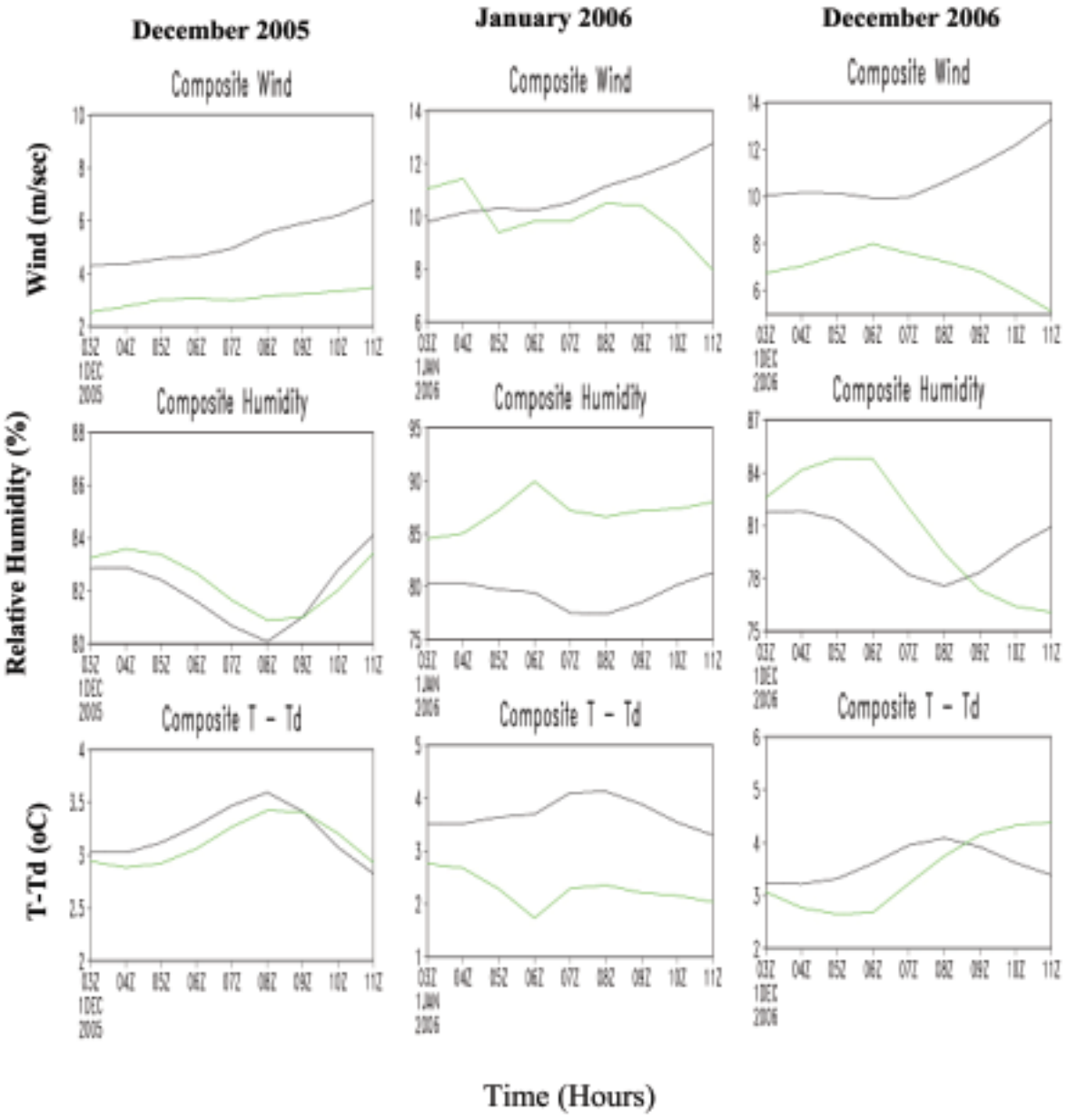

Figure 1. Composites of area-averaged (1^0 X 1^0 around 77.5^0E, 27^0N) hourly meso-scale forecasts for foggy (green dotted line) and non-foggy days (black solid line), showing average differences in the forecasts for and non-foggy days. The composites are created by averaging the forecasts separately over the days with fog and no fog.

A clear necessity to deal with the problem of fog is accurate and advance forecast with adequate resolution. For fog forecasts to be effective in an operational environment, they must provide accurate, quantitative estimates of onset, duration, ceiling and visibility with sufficiently high spatial and temporal resolution. Accurate and advance forecast of fog, however, continues to be a scientific challenge. One reason for this is that formation and the dynamics of fog depend on a combination of dynamical condition that are themselves difficult to predict. Further, the conventional meso-scale forecasts from a dynamical model need to be included in a calibrated model of visibility, which also depends on local conditions, aerosols etc.

With its emphasis on an integrated outreach programme that takes its scientific results from the lab to the people, CSIR has decided to develop the fog forecasting platform as a CSIR-Industry synergy.

synergy also ensures that the programme is developed in an industry-friendly way, and is eventually self-sustaining and revenue generating; An Agreement with the Industrial Partner covering these aspects, was signed following due procedures.

The Forecast Engine is a combination of High Performance Computing, new generation of dynamical meso-scale models, advanced data analysis and informatics. As mentioned earlier, forecast of fog also requires a model that combines various meteorological and other inputs in a quantitative and consistent manner to generate various fog related parameters. In the present case, a visibility model has been developed at C-MMACS based on a semi-empirical approach, which has been interfaced with a dynamical meso-scale model. The critical issue of calibration and validation of the forecast platform has been addressed from a number of angles, consistency, hindcast skill and sensitivity analysis. This is a difficult task due to lack of adequate data, especially over India. Validation must therefore be considered an on-going process.

While C-MMACS has set up the forecast engine, an Industrial Partner has converted this forecast platform to an industry compatible facility; the strategy is to develop the forecast platform in such a way so that it can be run in an operational manner in an industrial environment. The Industrial Partner had also carried out a preliminary study of market potential and market growth. These studies indicate considerable scope for commercial fog forecasts not only in the air traffic sector but also in road, rail and shipping industries, in India and abroad.

The facility has been functioning for Delhi since November 2005, with a web-based user interface (www.wecis.biz). Presently the forecasts are provided free on request as a part of testing and validation. Other fog-prone airports will be included in a phased manner. Once fully in place for one location, such a forecast platform will provide a scalable, multi-purpose forecast platform to include other important parameters such as heavy rainfall, flash floods and others.

The forecasts for the winter of 2005-06, communicated to a number of scientists for post-forecast validation, have been fairly accurate with only three misses and two (marginal) false warnings. However, the previous winter has had relatively fewer foggy days and more validation, including other locations, is necessary. An on-site validation, through a meso-scale observation network is already under implementation.

P Goswami